

Application of Phase Images for Estimation of Peritoneal Macrophages State

Alexander I. Yusipovich¹, Adil A. Bayzhumanov¹, Tatiana A. Kazakova¹, Alexander A. Cherkashin¹,
Tatiana R. Kamaletdinova¹, Sergey K. Pirutin¹, Natalia O. Rozhkova¹ & Georgy V. Maksimov¹

¹ Biological Faculty of M.V. Lomonosov Moscow State University, Moscow, Russian Federation

Correspondence: Alexander I. Yusipovich, Biological Faculty of M.V. Lomonosov Moscow State University, Moscow, Russian Federation. Tel: 7-495-939-1966. E-mail: brindikova@gmail.com

Received: February 26, 2015 Accepted: March 1, 2015 Online Published: September 30, 2015

doi:10.5539/ijb.v7n4p53

URL: <http://dx.doi.org/10.5539/ijb.v7n4p53>

Abstract

Procedure based on phase images obtained by the method of Laser Interference Microscopy (LIM) for detection of number non-activated, activated and dead isolated peritoneal macrophages in a sample *in vitro* was provided. The phase images provide quantitative estimates of the optical path difference (OPD) in each point of object. The OPD varies with cell thickness and concentration of cellular substances. Therefore, it provides useful information on cell structure, localization of subcellular structures, local concentrations of substances and dry mass of cell. In these work we propose a new assay for estimation a number of non-activated, activated and dead isolated peritoneal macrophages in a sample *in vitro* based on cell phase images. The results were compared with phagocytic index, which was evaluated using latex beads, and the percentage of cells with damaged membranes (dead cells). It was shown that with increasing time after the isolation, the percentage of dead macrophages estimated by LIM was similar to that of the cells with damaged membranes. However, the percentage of activated cells calculated using latex beads exceeded the percentage calculated using the phase images significantly.

Keywords: peritoneal macrophages, phase image, Laser Interference Microscopy (LIM)

1. Introduction

Various methods of interference microscopy has recently become rather popular in studies of cell morphology (e.g. (Barer, 1957; Byrne et al., 2008; Dunn, 1998; Marquet et al., 2015; Tychinsky & Tikhonov, 2010; Vishnyakov & Levin, 1998)). Interference microscopy and some noninterferometric methods (e.g. Curl et al., 2006; Roma et al., 2014) can provide quantitative estimates of the optical path difference (OPD) in each point of cell (phase images). The OPD varies with cell thickness and concentration of cellular substances. Therefore, it provides useful information on cell structure, localization of subcellular structures, local concentrations of substances and dry mass of cell. There are a lot of various type of cell were estimated using different methods of interference microscopy: erythrocytes (see e.g. Popescu et al., 2005; Popescu et al., 2006; Rappaz et al., 2007; Rappaz et al., 2008; Rappaz et al., 2009; Yusipovich, I et al., 2009; Yusipovich et al., 2011), fibroblasts (Dunn & Zicha, 1995), lymphocytes (Tychinsky et al., 2012), neurons (Rappaz et al., 2005; Yusipovich et al., 2006), nerve fibers (see e.g. Bibineyshvili et al., 2013; Brazhe et al., 2008; LaPorta & Kleinfeld, 2012; Maksimov et al., 2001), mast cells (Bondarenko et al., 2013), any microbiological objects (Tychinskii et al., 2007; Yusipovich et al., 2012; Zhurina et al., 2013) and others. In these work we propose a new assay for estimation a number of non-activated, activated and dead isolated peritoneal macrophages in a sample *in vitro* based on cell phase images. It was shown that activation of macrophages is accompanied by an increase of cell area, a minor (less than 10%) decrease in macrophage dry mass, and pronounced decrease in cell mass in case of cell death (Zagubizhenko et al., 2012). This helped us to distinguish the populations of non-activated, dead and activated macrophages.

2. Materials and Methods

2.1 Isolation of Macrophages

Macrophages were removed from the peritoneal cavity of male Wistar outbred rats, according to a standard procedure (Akhalya et al., 2006) with modifications. Suspension of peritoneal cells was layered over 30% Ficoll DL-400 (Sigma, USA) in PBS buffer (145 mM NaCl, 2,7 mM KCl, 2 mM KH₂PO₄, 4,6 mM Na₂HPO₄, 1 mg BSA per ml, 5 mM D-glucose, 1 mM CaCl₂, pH 7,4). Macrophages were separated by centrifugation at 3000 g for 30

min at 4°C. The cell fraction was carefully collected using Pasteur pipette at the interface between the buffer and Ficoll. Then the cell fraction was transferred to a 10 ml red cell lysing solution (201 mM NH₄Cl, 12.5 mM KHCO₃, 1.6 mM EDTA) and the suspension was centrifuged at 500 g for 5 min at 4°C. Supernatant was decanted, then purified macrophages were suspended in PBS buffer (pH 7.4). Experimental samples contained adherent cells only.

2.2 Macrophage Fraction Purity

Purity of macrophage fraction was controlled visually. The suspension of isolated peritoneal macrophages (25 µl) was placed on a slide. After complete desiccation of the sample, the fixed cells were stained accordingly to Romanowsky-Giemsa technique (Strober, 2001). Staining of the samples showed that only macrophages and their precursors (more than 99%) were present in this fraction.

2.3 Thawing Frozen (Dead) Cells Preparation

Cells obtained from the animals were placed in ice-cold HEPES buffer used for isolation of macrophages and frozen during 24 h at -84°C. Then cell specimens were fixed in two hours after defreezing, which was carried out without any special procedures preventing cell damage.

2.4 Cell Fixation

The macrophage suspension was placed on a mirror glass slide and fixed by glutaraldehyde solution (Serva, Germany) (Bondarenko et al., 2013). The samples were incubated for 1 hour at room temperature. Final concentration of glutaraldehyde was 2.5%. After incubation samples were rinsed with distilled water and dried in the air. In an hour before measurements, 10 µl glycerin solution (Sigma Aldrich, USA) mixed with distilled water at a ratio of 1:1 (by volume) was applied to the samples, then samples were covered with cover glasses.

2.5 Incubation of Cells with Latex Beads

Addition of latex beads (to assess the level of cell activation) was made immediately after placing the cell suspension on mirror glass slide (the final concentration of granules was 0.0025% by volume) (Figure 1a). The percentage of living activated cells in the sample (phagocytic index PI) was calculated as ratio of the fraction of cells containing at least one bead to total cell number, also the value of beads per cell (the phagocytic number PN) was estimated (Shirshv et al., 2000).

2.6 The Percentage of Cells with Damaged Membranes (Dead Cells) Detection

The percentage of cells with damaged membranes (dead cells) was estimated using ethidium bromide in final concentration 5 µg/ml (Serva) (Dankberg & Persidsky, 1976; Turovetskii et al., 1994). The cell damage was calculated as a ratio of the number of damaged cells to total cell number. Typical images of stained cells are shown on Figure 1b.

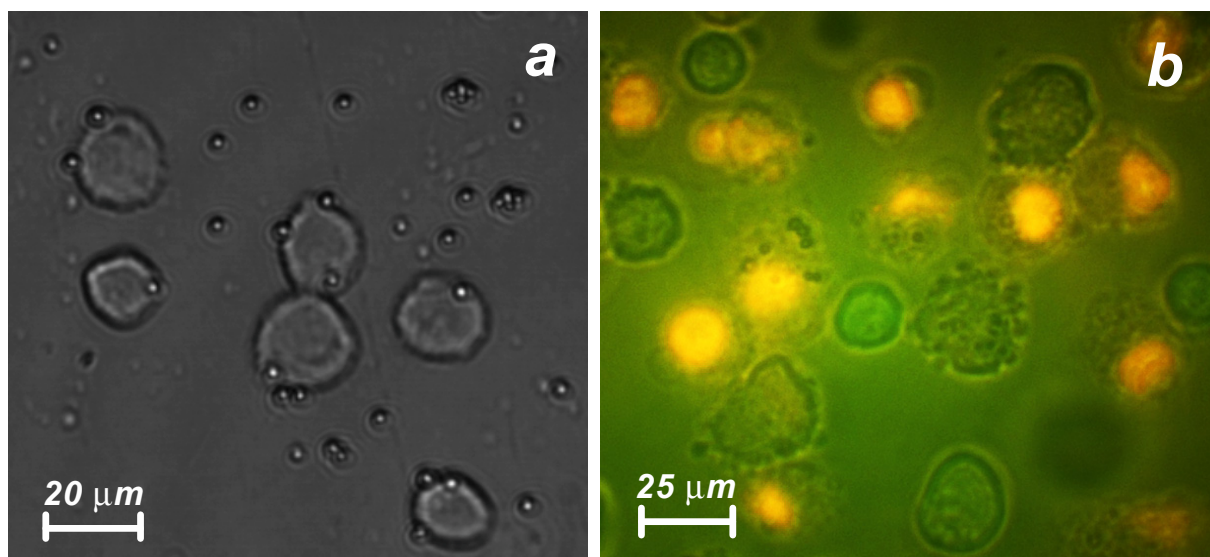


Figure 1. Typical image of cells incubated with latex beads (a) and stained by ethidium bromide, final concentration 5 µg/ml (b)

2.7 LIM Theory

The LIM is based on the measurements of the local phase of light wave reflected by the objects.

Laser beam is split into two, one of which (in case of transparent or semitransparent biological samples) travels through the object which changes its wave phase. The other beam is used as a reference and does not pass through the object. Superposition of the two beams results in the fringe pattern on the detector due to interference between the object and reference beams. Thus LIM measures the optical path difference of the two beams (Yusipovich et al., 2006).

Phase image of an object is a distribution of entire OPD value in its 2D projection. In case of optically inhomogeneous cells (e.g. cells with nuclei like macrophages) the OPD value of each projection point (i), is a sum of OPD values of each optically homogenous media with refractive index n_i and thickness z_i , n_m – refractive index of surrounding solution, z – sum of all z_i (Yusipovich et al., 2009):

$$OPD_i = (n_1^i z_1^i + n_2^i z_2^i + \dots + n_n^i z_n^i) - n_m z \quad (1)$$

Using LIM one can calculate the dry mass of cell (amount of substances), m , (Yusipovich et al., 2009):

$$m = \frac{\rho}{(n - n_m)} OPD_{mean} S \quad (2)$$

where ρ is the specific density of the substance (for protein: 1.33-1.36 (Barer & Joseph, 1954)), n is the refractive index of substance (for proteins: 1.5-1.6 (Barer, 1954)), OPD_{mean} is the arithmetical mean of all OPD values in the cell, S is the cell area.

In case of homogeneous cells, (e.g., anuclear erythrocytes filled by hemoglobin), m calculated by formula (2) is a correct estimate of the cell dry mass. In most other cells containing substances with different refractive indices, m represents overall changes in amounts of the substance in the cell.

In this study we use the following parameters to access the macrophages' conditions:

Cell area (S) is an area of cell phase image corresponding to 2D cell projection. Changes in area of macrophages occur during their activation and death.

Mean OPD of cell (OPD_{mean}) is arithmetical mean of any OPD values in cell needed for calculation of the cell dry mass.

Cell dry mass (m) is calculated as a product of the experimentally measured cell area, OPD_{mean} and constants from formula (2). A significant decrease in dry mass comparing to the control data is mainly determined by release of substances from the cell. The basic component of fixed cells is presumably proteins with specific density 1.36 g/cm³ and refractive index 1.56. The value n_m (the refractive index of mixture of glycerol and water in 1:1 volume ratio) was 1.404.

2.8 Phase Imaging

Imaging was performed using an automated interference MIA 1 microscope, developed at All Russian Scientific Research Institute for Optical and Physical Measurements (Moscow, Russia) (Minaev & Yusipovich, 2012; Yusipovich et al., 2011). The vertical sensitivity for each measured pixel was not less than $\lambda/200$ and the lateral resolution was not less than 0.5 μm . The phase imaging, calculation of area and mean values of OPD in cells were performed using Fiji image processing package (Schindelin et al., 2012).

2.9 Statistical Analysis

Subsequent statistical analysis was performed using the software package Statistica 8.0. Statistical significance was calculated by the t -test ($p < 0.05$). The presented data are mean values in each sample over all experimental animals. The number of animals used in our experiments is shown in Figure and Table captions. The number of cells analyzed in each sample exceeded 100. The regression analysis (third-order polynomial approximation, upper and lower 95% Prediction limits) for estimation of live and dead macrophages was also performed using the Statistica 8.0 software.

3. Results

In the first series of experiments the dynamics of LIM phase parameters was investigated (Table.1). The LIM measurements were done on fixed macrophages in 5, 60 and 120 min after isolation. The samples fixed in 5 min after isolation were taken as control.

Table 1. The values of macrophages LIM parameters (N=9)

Time after isolation, min	5	60	120	Dead cell
Area, μm^2	51,1 \pm 14,2	56,2 \pm 19,6	75,6 \pm 19,96*	104,0 \pm 33,6*
OPD _{mean} , nm	252,9 \pm 41,5	168,9 \pm 46,0*	133,4 \pm 27,2*	43,0 \pm 14,2*
Dry mass, pg	78,6 \pm 26,8	65,8 \pm 31,5*	69,1 \pm 21,8*	22,3 \pm 10,0*

The data shown is mean \pm standard deviation.

*significant difference compared to control (5 minutes in Table), values were calculated using the t-test at $p < 0.05$.

In general, cell area increased and OPD_{mean} and dry mass decreased over time. These data are in good agreement with the concept that cell activation is accompanied by an increase in cell area and decline in its dry mass (see, e.g., (Zagubizhenko et al., 2012)). It was also found that changes in cellular membrane and substance leakage into external medium lead to increase in cell area and decrease in OPD_{mean} and dry mass.

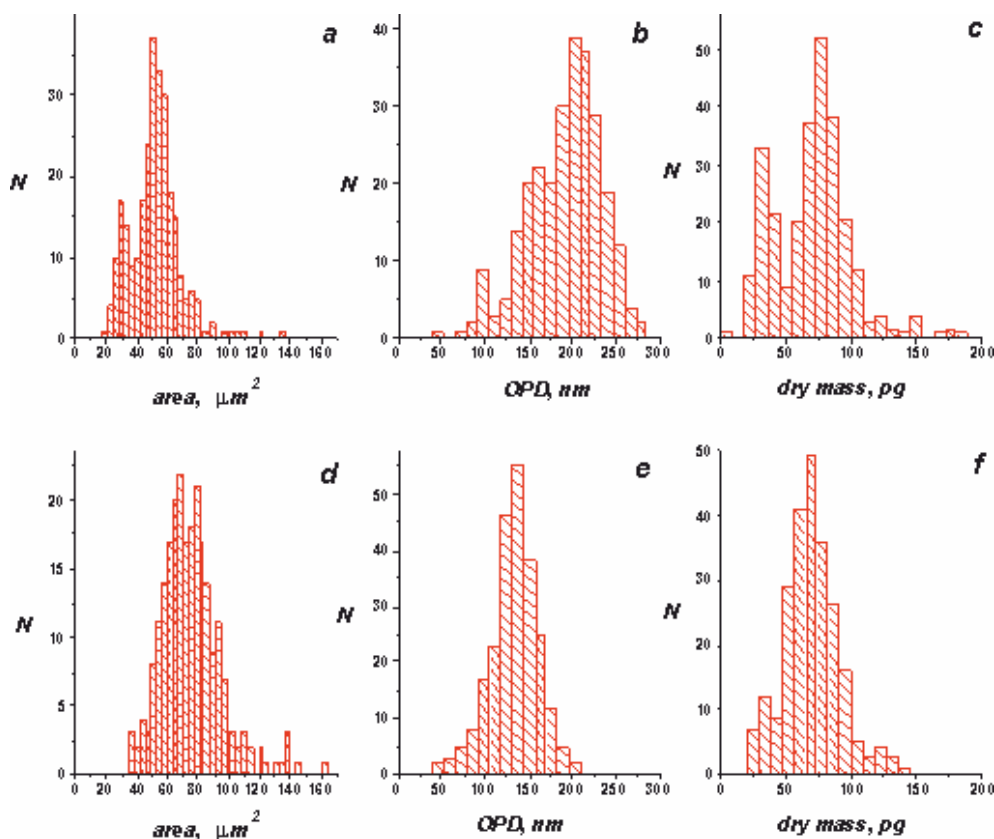


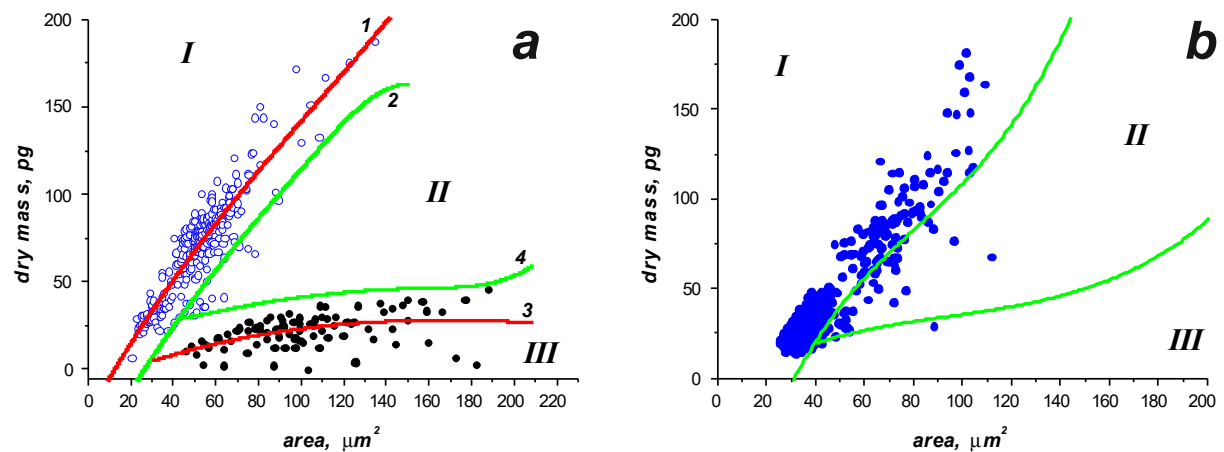
Figure 2. Typical bar charts of phase image parameters of macrophages after 5 (a, b, c) and 120 (d, e, f) min after isolation. a, d – cell areas; b, e – cell OPD_{mean} values; c, f – dry mass

The observed changes in the measured parameters may depend on the presence of both activated and dead cells. Figure 2 (a and c) show that population of macrophages was inhomogeneous. Figure 2 a and c show bimodal distributions of cell areas and dry mass, respectively. The first fraction is characterized by an average cell area $\sim 30 \mu\text{m}^2$, OPD_{mean} $\sim 160 \text{ nm}$, and dry mass of $\sim 30 \text{ pg}$. The second fraction has average cell area $\sim 50 \mu\text{m}^2$, OPD_{mean} $\sim 200 \text{ nm}$, and dry mass $\sim 80 \text{ pg}$. Presumably, these two fractions could be monocytes and mature macrophages, respectively. This hypothesis is confirmed by Romanowsky-Giemsa dyeing specific for macrophages and their precursors, the monocytes. The dimensions of both fractions of cells in samples change in time, which is evidenced by alterations in the form of distributions (Figure 2).

However, special methods and algorithms are needed to determine the percentage of active, inactive and dead cells.

3.1 Assay for Inactivated, Activated, and Dead Macrophages

The regression analysis was used to distinguish between the alive and dead cells. For this assay we used cells obtained from a single animal, to avoid possible morphological difference of cells between animals. Control samples fixed in 5 min after cell separation were used as an estimate of inactivated cells. The thawing cells were used as an estimate of dead cells.



The coefficients for third-order polynomials approximating the experimental data ($y=A+B_1x+B_2x^2+B_3x^3$)

Parameter	Inactivated	Dead
A	-26.46463	-8.9129
B ₁	2.19482	0.51114
B ₂	-0.00747	-0.00215
B ₃	$2.34131 \cdot 10^{-5}$	$2.49374 \cdot 10^{-6}$

Figure 3. Examples of boundary plots of characteristic regions used to distinguish dead, inactive, and active macrophages (a). Macrophages fixed in 5 minutes after isolation (**open circles**) represent a control population. Defrosting macrophages without any special procedures (**closed circles**) represent dead cells. Lines **1** and **3** are the third-order polynomials which approximate experimental data for the control and dead cells, respectively (the values of polynomial coefficients shown in **Table**). Line **2** is a lower 95% prediction limit for inactivated cells, it was used as a boundary between the inactive and other macrophages; line **4** is an upper 95% prediction limit for dead cells, which was used as a boundary between the dead macrophages and other cells. Areas **I**, **II** and **III** are the regions of inactivated, activated, and dead macrophages, respectively

Example of calculation of inactivated, activated, and dead macrophages in sample (b). I, II, and III are the regions of inactivated, activated, and dead macrophages, respectively. The number of inactivated, activated, and dead macrophages are 495, 42, and 1, respectively.

The fractions of inactivated, activated and dead macrophages in samples were estimated by measuring the area and dry mass. The experimental phase images were analysed using a plot of dry masses against the cell area (Figures 3). Then boundaries of regions occupied by dead and inactivated cells were defined (see Figure 3a). The determination of boundaries on x,y-plot was performed according to the following algorithm: the experimentally measured values of the control and dead macrophages were approximated by a third-order polynomial, then the estimated lower 95% prediction limit for inactivated cells was used as a boundary between the inactive and other macrophages, and the upper 95% prediction limit for dead cells was used as a boundary between the dead macrophages and other cells. When these boundaries are plotted, the characteristic regions were used to evaluate the number and percentage of non-activated, activated and dead cells in other samples of macrophages taken from the same animal. An example of this procedure is shown in Figure 3b. Typical images of inactivated, activated, and dead macrophages are shown in Figure 4. Boundary detection was performed only for (control, dead and unknown type) macrophages isolated from the same animal.

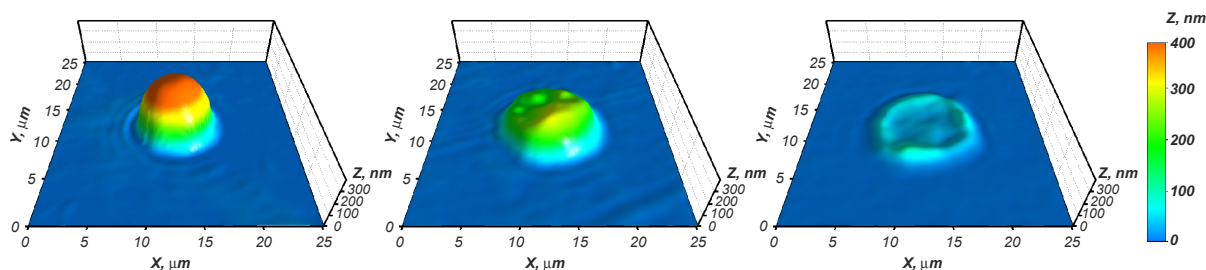


Figure 4. Typical phase images of an inactivated (left), activated (middle), and dead (right) macrophages

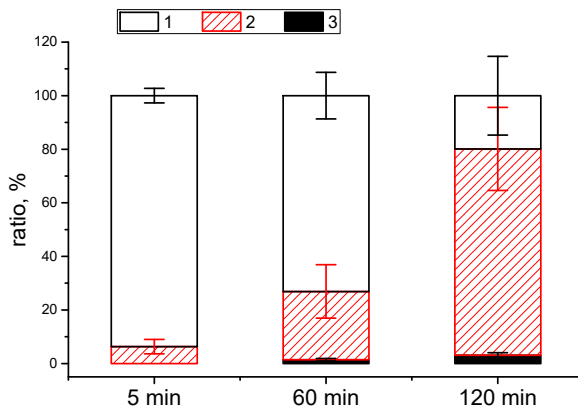


Figure 5. The ratio of inactivated (1), activated (2), and dead (3) macrophages, calculated from phase images (N=9). The data was shown as mean ± standard deviation

The percentages of inactivated, activated, and dead macrophages calculated from cell populations fixed in 5, 60 and 120 min after separation are presented on Figure 5. Over the time the amount of activated macrophages increases drastically while the number of inactivated macrophages declines. However, the percentage of dead cells increased only insignificantly.

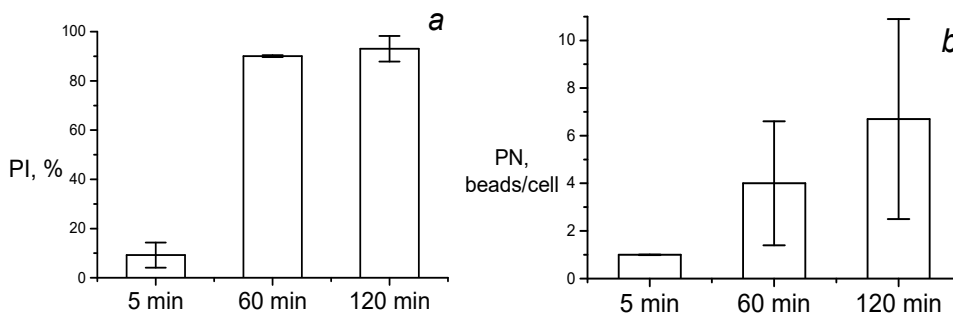


Figure 6. Phagocytic index, PI, (a); and phagocytic number, PN, (b). The data shown is mean ± standard deviation (N=6)

3.2 Estimation of Activated Macrophage Fraction using Latex Beads

Along with fixation of cells and LIM experiments phagocytic activity of live macrophages was estimated in the same samples. Immediately after isolation of macrophages latex beads were introduced into the samples obtained from one and the same animal Then we estimated PI and PN independently using conventional microscopy, as well as area and amount of substances in fixed macrophages, which contained beads, using phase images obtained in equal time intervals. Phase images did not use for detection of PI and PN because the phagocytosed latex beads and native granules in cells had similar OPD and could not be properly distinguished on the phase images.

Moreover, the percentage of nonactivated, dead and activated cells was not significantly different between the macrophages in the presence of latex beads and in case of macrophages without beads.

It was shown PI increased drastically in 60 minutes after separation, whereas PN grew gradually.

3.3 Estimation of Macrophage Fraction with Damaged Membranes (Dead) by Staining with Ethidium Bromide

To compare the percentage of dead cells by an independent technique we stained samples of macrophages with ethidium bromide in 0, 60 and 120 mi after isolation (Figure 7). The fraction of dead cells increased drastically in two hours after cell separation. At the same time dead cell fraction, calculated by ethidium bromide assay was not significantly different from the corresponding fraction obtained from phase images (T-test, $p < 0.05$).

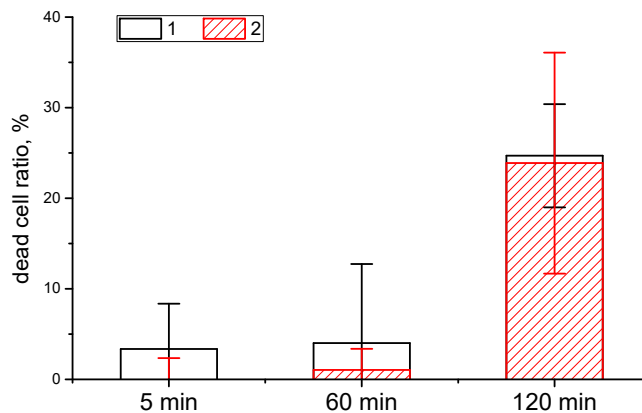


Figure 7. The fraction of dead cells calculated using LIM (1) and ethidium bromide staining (2) (N=6).

4. Discussion

The main aim of the study was to compare different approaches and demonstrate efficiency of LIM for biological research. It was shown that there is no significant difference between the estimates of calculation of dead cells fraction obtained from the LIM data and conventional (ethidium bromide assay) technique. This suggests the possibility of LIM application for assaying the fraction of dead cells in samples of macrophages without dyeing. However, we found some differences between the fraction of activated macrophages calculated by LIM data and latex beads. Moreover, the fraction of activated macrophages after cell isolation, calculated over time using latex beads, exceeded considerably the same parameter calculated by LIM. Consequently, the percentage of activated and inactivated macrophages determined by LIM in 1 hour after separation, closely corresponded to the value of PI (may be all macrophages are practically stucked around beads). It should be kept in mind that when optical microscope could not easily distinguish between granules adsorbed on the cell surface and those phagocytosed by macrophages, which leads to overestimation of PI and PN values. We assume that beads are at first adsorbed on macrophage surface and then, over the time, they are taken up into the cell. Thus, within first 60 minutes PI and PN reflect the absorption of granules on the surface of macrophages, and only later on the absorption of these beads by cells could take place. It is also possible that some delay in activation of macrophages revealed by LIM is determined by the fact that parameters measured by LIM reflect morphological changes during the activation or other processes as compared to PI and PN dynamics.

It is well known that macrophages are involved not only in phagocytosis, but are also a source of active mediators, which are emitted by exocytosis into the intercellular space. They can affect the functional activity of the neighboring cells through a paracrine interaction. Since this process is related to activation of trans-membrane receptors, changes in the structure of some proteins, and initiation of the cascade mechanism of signal transduction, a definite time seems to be required for visualization of this process. Apparently using LIM we registered only those processes which were associated with the mediator activity of macrophages.

References

- Akhalaya, M. Y., Baizhumanov, A. A., & Graevskaya, E. E. (2006). Effects of taurine, carnosine, and casomorphine on functional activity of rat peritoneal mast cells. *Bulletin of Experimental Biology and Medicine*, 141, 328-330. <http://dx.doi.org/10.1007/s10517-006-0162-8>

- Barer, R. (1957). Refractometry and Interferometry of Living Cells. *Journal of the Optical Society of America*, 47(6), 545-556. <http://dx.doi.org/10.1364/JOSA.47.000545>
- Barer, R., & Joseph, S. (1954). Refractometry of Living Cells. Part I. Basic Principles. *Quarterly Journal of Microscopical Science*, 95, 399-423.
- Bibineyshvili, E. Z., Rodionova, N. N., Yusipovich, A. I., & Maksimov, G. V. (2013). Modifications of Protein-Lipid Interactions in Nerve Fiber Myelin: Effects on Nerve Fiber Morphology. *Biologicheskie Membrany*, 30(2), 142-146. <http://dx.doi.org/10.7868/S0233475513020023>
- Bondarenko, N. S., Yusipovich, A. I., Kovalenko, S. S., Kopylova, G. N., Umarova, B. A., Graevskaya, E. E., & Maksimov, G. V. (2013). Application of laser interference microscopy (LIM) for investigation of the protective effect of prolyl-glycyl-proline (Pro-Gly-Pro) on mast cells. *Biochemistry (Moscow) Supplement Series A: Membrane and Cell Biology*, 7(3), 222-227. <http://dx.doi.org/10.1134/S1990747813030033>
- Brazhe, A. R., Brazhe, N. A., Rodionova, N. N., Yusipovich, A. I., Ignatyev, P. S., Maksimov, G. V., ... & Sosnovtseva, O. V. (2008). Non-invasive study of nerve fibres using laser interference microscopy. *Philosophical Transactions of the Royal Society of London A: Mathematical, Physical and Engineering Sciences*, 366(1880), 3463-3481. <http://dx.doi.org/10.1098/rsta.2008.0107>
- Byrne, G. D., Pitter, M. C., Zhang, J., Falcone, F. H., Stolnik, S., & Somekh, M. G. (2008). Total internal reflection microscopy for live imaging of cellular uptake of sub-micron non-fluorescent particles. *Journal of Microscopy*, 231, 168-179. <http://dx.doi.org/10.1111/j.1365-2818.2008.02027.x>
- Curl, C. L., Bellair, C. J., Harris, P. J., Allman, B. E., Roberts, A., Nugent, K. A., & Delbridge, L. M. (2006). Single cell volume measurement by quantitative phase microscopy (QPM): a case study of erythrocyte morphology. *Cellular Physiology and Biochemistry*, 17(5-6), 193-200. <http://dx.doi.org/10.1159/000094124>
- Dankberg, F., & Persidsky, M. D. (1976). A test of granulocyte membrane integrity and phagocytic function. *Cryobiology*, 13, 430-432. [http://dx.doi.org/10.1016/0011-2240\(76\)90098-5](http://dx.doi.org/10.1016/0011-2240(76)90098-5)
- Dunn, G. A. (1998). Transmitted-light interference microscopy: a technique born before its time. *Proceedings of the Royal Microscopical Society*, 33, 189-196.
- Dunn, G. A., & Zicha, D. (1995). Dynamics of fibroblast spreading. *Journal of Cell Science*, 108(Pt 3), 1239-1249.
- LaPorta, A., & Kleinfeld, D. (2012). Interferometric detection of action potentials. *Cold Spring Harbor Protocols*, 2012(3), 307-311. <http://dx.doi.org/10.1101/pdb.ip068148>
- Maksimov, G. V., Nikandrov, S. L., Lazareva, E. S., Tychinskii, V. P., & Rubin, A. B. (2001). A study of demyelination of nerve fibers using dynamic phase contrast microscopy. *Bulletin of Experimental Biology and Medicine*, 131(5), 457-460. <http://dx.doi.org/10.1023/A:1017923915116>
- Marquet, P., Rappaz, B., & Pavillon, N. (2015). Quantitative Phase-Digital Holographic Microscopy: A New Modality for Live Cell Imaging. *New Techniques in Digital Holography* (pp. 169-217). Hoboken, NJ, USA: John Wiley & Sons, Inc. <http://dx.doi.org/10.1002/9781119091745.ch5>
- Minaev, V. L., & Yusipovich, A. I. (2012). Use of an automated interference microscope in biological research. *Measurement Techniques*, 55, 839-844. <http://dx.doi.org/10.1007/s11018-012-0048-2>
- Popescu, G., Badizadegan, K., Dasari, R. R., & Feld, M. S. (2006). Observation of dynamic subdomains in red blood cells. *Journal of Biomedical Optics*, 11(4), 040503. <http://dx.doi.org/10.1117/1.2221867>
- Popescu, G., Ikeda, T., Best, C. A., Badizadegan, K., Dasari, R. R., & Feld, M. S. (2005). Erythrocyte structure and dynamics quantified by Hilbert phase microscopy. *Journal of Biomedical Optics*, 10(6), 060503. <http://dx.doi.org/10.1117/1.2149847>
- Rappaz, B., Barbul, A., Emery, Y., Korenstein, R., Depeursinge, C., Magistretti, P. J., & Marquet, P. (2007). Erythrocytes volume and refractive index measurement with a digital holographic microscope. *SPIE--The International Society for Optical Engineering*, 6445, 644509. <http://dx.doi.org/10.1117/12.700463>
- Rappaz, B., Barbul, A., Emery, Y., Korenstein, R., Depeursinge, C., Magistretti, P. J., & Marquet, P. (2008). Comparative study of human erythrocytes by digital holographic microscopy, confocal microscopy, and impedance volume analyzer. *Cytometry A*, 73(10), 895-903. <http://dx.doi.org/10.1002/cyto.a.20605>
- Rappaz, B., Barbul, A., Hoffmann, A., Boss, D., Korenstein, R., Depeursinge, C., Magistretti, P. J., & Marquet, P. (2009). Spatial analysis of erythrocyte membrane fluctuations by digital holographic microscopy. *Blood Cells Mol. Dis.*, 42(3), 228-232. <http://dx.doi.org/10.1016/j.bcmd.2009.01.018>

- Rappaz, B., Marquet, P., Cuche, E., Emery, Y., Depeursinge, C., & Magistretti, P. (2005). Measurement of the integral refractive index and dynamic cell morphometry of living cells with digital holographic microscopy. *Optics Express*, *13*, 9361-9373. <http://dx.doi.org/10.1364/OPEX.13.009361>
- Roma, P. M. S., Siman, L., Amaral, F. T., Agero, U., & Mesquita, O. N. (2014). Total three-dimensional imaging of phase objects using defocusing microscopy: Application to red blood cells. *Applied Physics Letters*, *104*(25), 251107. <http://dx.doi.org/10.1063/1.4884420>
- Schindelin, J., Arganda-Carreras, I., Frise, E., Kaynig, V., Longair, M., Pietzsch, T., ... Cardona, A. (2012). Fiji: an open-source platform for biological-image analysis. *Nature Methods*, *9*, 676-682. <http://dx.doi.org/10.1038/nmeth.2019>
- Shirshev, S. V., Lyalina, O. G., & Zamorina, S. A. (2000). Role of potassium ions in monocyte-regulating effects of chorionic gonadotropin. *Bull Exp Biol Med*, *130*(5), 1099-1101. <http://dx.doi.org/10.1007/BF02688190>
- Strober, W. (2001). Wright-Giemsa and nonspecific esterase staining of cells. *Curr. Protoc. Immunol. Appendix*, *3*. <http://dx.doi.org/10.1002/0471142735.ima03cs21>
- Turovetskii, V. B., Zolotilin, S. A., Sarycheva, N. I., Kalikhevich, V. N., & Kamenskii, A. A. (1994). Effect of tuftsin on the functional activity and intracellular pH of murine peritoneal macrophages. *Bulletin of Experimental Biology and Medicine*, *117*, 267-269. <http://dx.doi.org/10.1007/BF02444159>
- Tychinskii, V. P., Nikolaev, Y. A., Lisovskii, V. V., Kretushev, A. V., Vyshenskaya, T. V., Mulykin, A. L., ... El'Registan. (2007). Research on the early stages of spore germination in *Bacillus licheniformis* using dynamic phase microscopy. *Microbiology*, *76*(2), 164-171. <http://dx.doi.org/10.1134/S0026261707020063>
- Tychinsky, V. P., & Tikhonov, A. N. (2010). Interference microscopy in cell biophysics. 1. Principles and methodological aspects of coherent phase microscopy. *Cell Biochem. Biophys*, *58*(3), 107-116. <http://dx.doi.org/10.1007/s12013-010-9114-z>
- Tychinsky, V. P., Kretushev, A. V., Vyshenskaya, T. V., & Shtil, A. A. (2012). Dissecting eukaryotic cells by coherent phase microscopy: quantitative analysis of quiescent and activated T lymphocytes. *Journal of Biomedical Optics*, *17*(7), 0760201-0760208. <http://dx.doi.org/10.1117/1.JBO.17.7.076020>
- Vishnyakov, G., & Levin, G. (1998). Linnik tomographic microscope for investigation of optically transparent objects. *Measurement Techniques*, *41*, 906-911. <http://dx.doi.org/10.1007/BF02503961>
- Yusipovich, A. I., Parshina, E. Y., Brysgalova, N. Y., Brazhe, A. R., Brazhe, N. A., Lomakin, A. G., ... Maksimov, G. V. (2009). Laser interference microscopy in erythrocyte study. *Journal of Applied Physics*, *105*, 102037-1-102037-7. <http://dx.doi.org/10.1063/1.3116609>
- Yusipovich, A. I., Berestovskaya, Y., Shutova, V. V., Levin, G. G., Gerasimenko, L. M., Maksimov, G. V., & Rubin, A. B. (2012). New possibilities for the study of microbiological objects by laser interference microscopy. *Measurement Techniques*, *55*(3), 351-356. <http://dx.doi.org/10.1007/s11018-012-9963-5>
- Yusipovich, A. I., Novikov, S. M., Kazakova, T. A., Erokhova, L. A., Brazhe, N. A., Lazarev, G. L., & Maksimov, G. V. (2006). Peculiarities of studying an isolated neuron by the method of laser interference microscopy. *Quantum Electronics*, *36*, 874-878. <http://dx.doi.org/10.1070/QE2006v036n09ABEH013408>
- Yusipovich, A. I., Zagubizhenko, M. V., Levin, G. G., Platonova, A., Parshina, E. Y., Grygorzcyk, R., ... Orlov, S. N. (2011). Laser interference microscopy of amphibian erythrocytes: impact of cell volume and refractive index. *Journal of Microscopy*, *244*, 223-229. <http://dx.doi.org/10.1111/j.1365-2818.2011.03516.x>
- Zagubizhenko, M. V., Yusipovich, A. I., Pirutin, S. K., Minaev, V. L., & Kudryashov, Y. (2012). Use of laser interference microscopy to study the state of UV(B)-irradiated mouse peritoneal macrophages. *Measurement Techniques*, *55*, 726-730. <http://dx.doi.org/10.1007/s11018-012-0028-6>
- Zhurina, M. V., Kostrikina, N. A., Parshina, E. Y., Strelkova, E. A., Yusipovich, A. I., Maksimov, G. V., & Plakunov, V. K. (2013). Visualization of the extracellular polymeric matrix of *Chromobacterium violaceum* biofilms by microscopic methods. *Microbiology*, *82*(4), 517-524. <http://dx.doi.org/10.1134/S0026261713040164>

Copyrights

Copyright for this article is retained by the author(s), with first publication rights granted to the journal.

This is an open-access article distributed under the terms and conditions of the Creative Commons Attribution license (<http://creativecommons.org/licenses/by/3.0/>).